J Appl Electrochem (2011) 41:1021–1032
DOI 10.1007/s10800-011-0298-8

ORIGINAL PAPER

Nonlinear frequency response analysis for the diagnosis of carbon monoxide poisoning in PEM fuel cell anodes

Thomas Kadyk · Richard Hanke-Rauschenbach · Kai Sundmacher

Received: 26 November 2010 / Accepted: 21 March 2011 / Published online: 5 April 2011

Abstract Anodic CO poisoning of a PEMFC was analysed by nonlinear frequency response analysis (NFRA) in a differential H_2/H_2 cell. This special experimental setup excluded potential masking effects, emphasised the main mechanism of CO poisoning and made a simplified modelling approach possible. The main features of CO poisoning were investigated by means of steady state polarisation, EIS and NFRA. The main characteristics of CO poisoning in the NFRA spectra can be used as a "fingerprint" for diagnostic purposes.

Keywords Polymer electrolyte membrane fuel cell · Nonlinear frequency response analysis · Higher order frequency response function · Carbon monoxide

List of symbols

a_{H_2O}	Activity of water, [0 … 1]
A	Amplitude, A m^{-2}
$b_{c/h}$	Tafel slope of CO or hydrogen electrooxidation, V
$b_{fc/fh}$	Ratio of desorption to adsorption rate constant for CO or hydrogen, [0 … 1]
$C_{DL,A/C}$	Anodic or cathodic double layer capacity, F m_{act}^{-2}
d_M	Thickness of the membrane, m
F	Faraday constant, 96485.3 A s mol^{-1}
$k_{ec/eh}$	Rate constant of CO or hydrogen electrooxidation, mol m_{act}^{-2} s^{-1}
$k_{fc/fh}$	Rate constant of CO or hydrogen adsorption, mol m_{act}^{-2} s^{-1}
i	Current density, A m^{-2}
p	Number of affected sites for Temkin adsorption
p_A	Pressure at the anode, Pa
$r_{CO/H}^{ads/des/ox}$	Rates of CO or hydrogen adsorption, desorption or oxidation, mol m_{act}^{-2} s^{-1}
R_M	Membrane resistance, $\Omega\, m_{geom}^{-2}$
U_{cell}	Cell voltage, V
$x_{CO/H}$	Mole fraction of CO or hydrogen, [0… 1]

Greek

$\delta(\Delta G_{CO})$	Variation of adsorption free energy between $\Theta_{CO} = 0$ and $\Theta_{CO} = 1$, J mol^{-1}
$\delta(\Delta E_H)$	Change in activation energy for hydrogen dissociative adsorption near CO occupied site, J mol^{-1}
ϵ	Roughness factor, $m_{act}^2\, m_{geom}^{-2}$
$\eta_{A/C}$	Anode or cathode overpotential, V
$\Theta_{CO/H}$	Coverage of catalyst with CO or hydrogen, [0 … 1]
Θ_{Pt}	Free active Pt catalyst sites, [0 … 1]
κ	Conductivity of the membrane, S m^{-1}
ρ	Molar area density of active sites, mol m_{act}^{-2}

Subscripts

0	Reference conditions
A	Anode
act	Active area
C	Cathode
CO	Carbon monoxide
eh	Electrooxidation of hydrogen
ec	Electrooxidation of carbon monoxide

T. Kadyk · R. Hanke-Rauschenbach (✉) · K. Sundmacher
Max Planck Institute for Dynamics of Complex Technical Systems, Sandtorstrasse 1, 39106 Magdeburg, Germany
e-mail: hanke-rauschenbach@mpi-magdeburg.mpg.de

T. Kadyk · K. Sundmacher
Otto-von-Guericke University Magdeburg, Universitätsplatz 1, 39106 Magdeburg, Germany

fh Adsorption of hydrogen
fc Adsorption of carbon monoxide
geom Geometric area
H Hydrogen
H_2O Water
Pt Platinum

Superscripts
ads Adsorption
des Desorption
ox Oxidation
red Reduction

1 Introduction

Fuel cells play an important role for the future energy supply because of their high efficiency and their possibility to use alternative, renewable energy sources. Especially polymer electrolyte membrane fuel cells (PEMFC) are of interest for many applications (e.g. mobile or automobile applications, decentralised electrical power supply) because of their low operation temperature, easy operation management, possibility for fast load changes and quick startup.

During the operation of PEMFCs several problems can lead to performance loss, e.g. defective water management can lead to dehydration of the proton conducting membrane or to flooding of the catalyst, gas diffusion layer or complete channels; fuel gas impurities like carbon monoxide can lead to poisoning of the catalyst and low gas flow rates can lead to fuel gas starvation in the flow field channel. Therefore, in situ methods for diagnosis are necessary for the operation management. Preferably, the electrical behaviour is used for diagnosis, because it is easily accessible for in situ measurement. For example, it can be easily implemented into the power electronics like DC/DC or DC/AC converters [1].

A commonly used technique for such a diagnosis is electrochemical impedance spectroscopy (EIS) [2–5], in which a small sinusoidal perturbation excites the system in a small, quasi-linear range around the working point. The resulting output signal is then analysed in a linear way. In the field of PEM fuel cells EIS has been widely used for diagnosis of e.g. water management [6, 7] or carbon monoxide poisoning [7], but it could be seen that there are operation conditions under which the spectra of different processes are similar and it can not be unambiguously distinguished between them, e.g. for the case of cathode flooding and CO poisoning [8] or for cell dehydration and CO poisoning [9]. A possible cause for such ambiguous spectra could be the linear analysis method of the EIS, which might not always be sufficient to adequately describe nonlinear systems like PEMFCs.

To overcome this problem a variety of nonlinear methods was established during the last decades. These can be divided into two classes. The first class is referred to as high amplitude AC voltammetry. It has been developed independently from Engblom et al. [10] and Gavaghan and Bond [11]. It extends the second order AC voltammetry which was developed by Smith in the 1960s [12]. In this technique, a sinusiodal potential of a single frequency and elevated amplitude is superimposed onto the linear or cyclic voltage sweep used in classical voltammetry.

The second class of nonlinear methods is based on high amplitude sinusiodal perturbation of the system around one steady operating point. In nonlinear electrochemical systems, the output signal is characterized by a DC rectification signal and the occurrence of higher harmonics. This second class of nonlinear methods can be divided into three subcategories: (1) methods dealing with the DC rectification (faradaic rectification; see [13] for a review); (2) methods analysing the higher harmonics (harmonic analysis; see [13–15] for reviews), e.g. faradaic distortion, harmonic impedance spectroscopy, electrochemical frequency modulation/intermodulation voltammetry, harmonic synthesis, total harmonic distortion analysis [16, 17] and nonlinear frequency response analysis [9, 18]; (3) methods analysing the amplitude dependence of the fundamental harmonics (nonlinear EIS, suggested by Darowicki [19–21]).

From these methods, nonlinear frequency response analysis (NFRA) is highly suitable for the analysis of PEM fuel cells because it is not tailored to one special model or mechanism but allows the analysis complex models and mechanisms. Additionally, with NFRA analytical solutions of modelled spectra are possible [18]. With this, problems with the numerical treatment, e.g. long computing times, numerical errors, solver problems etc., can be avoided. Recently, Bensmann et al. [18] noted that NFRA is similar to the method used by the Adler group [22, 23]. However, the mathematical background is different.

With NFRA, a moderately increased amplitude is used as an input signal. With this, the system can no longer be assumed to be linear around the working point but nonlinear distortions occur. These distortions can be analysed with a mathematical framework of Fourier transform and Volterra series approximation and so called higher order frequency response functions (HFRF) are obtained. The HFRF of first order is thereby identical to the EIS spectrum and describes the linear behaviour of the system around the working point. Additionally, HFRF of higher order contain information about the nonlinearities of the system. NFRA has been developed in the 1980 for the analysis of analogue electrical circuits [24] and successfully used for the investigation of adsorption systems (see [25] for a review)

and methanol oxidation kinetics [18]. One important result was the possibility to discriminate between different adsorption kinetic mechanisms [26, 25] and different methanol oxidation kinetics [18] based on the shape of the second order frequency response functions.

In a previous work [9], we used NFRA for the diagnosis of dehydration, flooding and CO poisoning in a complete PEMFC. Thereby, it was seen that the cases of dehydration and CO poisoning are of special interest because similar behaviour in the linear spectra was observed but differences in the nonlinear spectra of the second order were found. Therefore, in the current work the case of CO poisoning was chosen to be analysed separately. For such a detailed analysis a complete fuel cell with technical conditions and dimensions would be rather complex and the investigated process would be masked by other processes. Therefore, the current work investigates the case of anodic carbon monoxide poisoning in a specially designed experiment, in which the following masking effects are avoided: Slow cathodic oxygen reduction kinetics are avoided by operating the cell with hydrogen at the cathode, a well established method in literature [27–29]. Land-channel effects like starvation of oxygen under the ribs of the cathode as observed by Schneider et al. [30] are avoided in such an operation mode, because no consumption reaction takes place at the cathode, only a hydrogen evolution reaction. Additionally, along-the-channel effects like fuel gas starvation or CO accumulation are prevented by a cell design with differentially short channels.

With this, the system can be described by a simple model, which neglects spatial distributions and emphasises the main mechanisms of CO poisoning. Such a simplified model makes it possible to calculate the NFRA spectra numerically or even derive them analytically. With this, the influence of the modelled processes on the NFRA spectra can be analysed in detail. Domains in the spectra can be found which are sensitive to single processes. The knowledge of these domains makes an unambiguous diagnosis of the performance limiting processes possible.

In the following section, the experimental methods and materials as well as the NFRA analysis method will be described. An experimental analysis of the CO poisoning process will be given in Sect. 3 in form of polarization curves, electrochemical impedance spectroscopy and NFRA spectra. In Sect. 4 possibilities for a theoretical access to the NFRA spectra are depicted by adaption of Springer's model for anode CO poisoning [31] and simulation of the NFRA spectra with the original model parameters for the operation conditions used in the experiments. In the last section the results are summarised and final conclusions are drawn.

2 Experimental setup and NFRA method

In this section the preparation and conditioning of a differential H_2/H_2 cell is described. The instrumentation and procedures for the measurement of polarisation curves, EIS spectra and NFRA spectra are explained. Comments on the stability and reproducibility are made and the mathematical background for the calculation of the NFRA spectra is given.

All experiments were done with a PEM fuel cell consisting of Nafion®1035 as the polymer electrolyte membrane. The Nafion® membrane was prepared by boiling in 5% H_2O_2 solution for one hour at 90 °C, washing in hot water, boiling in 1 molar H_2SO_4 solution for two hours at 100 °C, washing in hot water and boiling in water for two hours. Deoinized water additionally filtered with a Millipore® purification system and an ohmic resistivity greater then 10 MΩ cm was used for all experiments.

The catalyst layer was spray painted onto the membrane. It consisted of Pt black from Alfa Aesar® with 10 wt% of Nafion®. The solvent for the spray painting process was water. The active area of the differential design was 1 cm^2 with a target Pt loading of 1 mg cm^{-2}. Due to the low overall Pt mass the target loading could only be prepared with high relative error and a large inaccuracy in the Pt loading was expected. Therefore, the mathematical model had to account for this inaccuracy, as will be explained in the next section.

After spraying of the catalyst layer it was dried at 120 °C and sintered onto the membrane at 130 °C for 30 min to ensure protonic conductivity between catalyst layer and membrane. The resulting catalyst layer covered an area of 1.6 mm × 63 mm, i.e. 1 cm^2 with a channel length of 1.6 mm.

The gas diffusion layer consisted of Toray paper TGP-H-060 hydrophobised with 15 wt% PTFE. Graphite flow field plates with 21 parallel flow channels with a width of 1.5 mm, depth of 2 mm and 2 mm ribs between them distributed the gases. Gold plated copper current collector plates provided the electrical connection and stainless steel plates braced the cell together by 12 screws fixed with a torque of 7 Nm.

The cell was run in a FuelCon Evaluator C test station at a temperature of 80 °C. The gases had flow rates of 200 ml min^{-1} on both sides in order to ensure a high overstoichiometry. They were humidified by bubbler bottles at 70 °C and kept 90 °C between the bubbler bottles and the cell in order to prevent condensation of the water. A Solartron 1286 potentiostat together with a Solartron 1250 frequency response analyser were used for the measurements.

The cell was initially conditioned by a method similar to that of Himanen et al. [29]. During the conditioning, the cell was operated in normal fuel cell mode with hydrogen at the anode and oxygen at the cathode. The current was increased stepwise from 0 to 1 A cm^{-2} in steps of 50 mA cm^{-2} with a duration of 20 min. After this, the cell was purged with nitrogen, anode and cathode were reversed and the procedure was repeated. This whole procedure was repeated three times until the cell performance was stable and the U–I curve was reproducible. After this, the cell was purged with nitrogen and the H_2/H_2 measurements were started.

Cell polarisation curves were taken by applying constant voltage steps from the open circuit voltage 0 to −0.9 V with 2 min duration, after which the measured current was stable and in steady state.

All EIS and NFRA spectra were taken in galvanostatic mode in order to control the reaction rates directly. If potentiostatic control would be used, especially in the case of NFRA, a high amplitude voltage signal could force very high currents to flow and the resulting faradaic rectification current could lead to enhanced degradation of the cell. This is prevented by galvanostatic control.

EIS spectra were measured at a working point of 0.1 A cm^{-2} (see Sect. 3 for a discussion of the working point selection) with an amplitude of 10 mA in the frequency range from 0.1 Hz to 10 kHz. For the measurement of NFRA spectra the same working point and frequency range were used. The excitation amplitude for the NFRA spectra was determined in a preliminary experiment: in order to use the simplified NFRA approach as described in [9], the amplitude must be large enough to be able to measure first and second harmonic but has to be so small that the third harmonic is negligible compared to the first harmonic and the fourth harmonic has to be negligible compared to the second harmonic. This restriction was fullfilled with an amplitude of 90 mA cm^{-2} in the measurements without CO on the anode and with an amplitude of 60 mA cm^{-2} in the measurements with 20 ppm and 100 ppm.

EIS and NFRA spectra were measured sequentially in one measurement cycle in the following way: the working point was reached with a slow ramp from 0 to 100 mA cm^{-2} with 1 mA cm^{-2} s^{-1}, then the cell was operated at the working point for 5 min to ensure that the voltage was stable. After this, an EIS spectrum was measured, then the cell was again operated for 5 min at constant current, an NFRA spectrum was measured and then the cell was again operated for 5 min at constant current. The measurement of the cell voltage during the operation phases at constant current made sure that the working point was stable during the measurement cycle. This measurement cycle was repeated three times in order to check and ensure a good reproducibility of the measurements.

The NFRA spectra were calculated from the measured higher harmonics according to the mathematical method described in Kadyk et al. [9] and Bensmann et al. [18]. If the amplitude of the input signal is carefully chosen in the described way, the output signal contains only a first and second harmonic. In this case the Volterra series consists of only two higher order frequency response functions $H_{1,0}$ and $H_{2,0}$, which can be calculated in the following way:

$$H_{1,0} = \frac{H_{q,I}(\omega, A)}{A} \tag{1}$$

$$H_{2,0} = 2\frac{H_{q,II}(\omega, A)}{A^2} \tag{2}$$

where $H_{q,I}$ and $H_{q,II}$ are the measured first and second harmonic quasi frequency response functions, which are obtained from the measurement as a set of complex numbers. They are functions of amplitude A and angular frequency $\omega = 2\pi f$ of the input signal.

3 Experimental results and discussion

The differential H_2/H_2 cell setup described in the previous section was used to analyse the main mechanism of CO oxidation without masking processes and effects. In the following section, the polarisation curve of the cell in normal PEMFC operation and in H_2/H_2 operation with different levels of CO poisoning on the anode are discussed. Afterwards, EIS spectra are shown and the main features of CO poisoning are explained. Subsequently, measured NFRA spectra are analysed and compared with EIS. The NFRA spectra reveal a fingerprint of the CO poisoning mechanism, which might be used for diagnosis as described in the last section.

In Fig. 1a the polarisation curve of the differential cell under normal fuel cell operation with oxygen on the cathode is shown. Cathode activation losses can be seen in the low current density region followed by a linear voltage decrease caused by membrane and ohmic resistances at increasing current density. High gas flow rates prevent limiting behaviour caused by fuel gas starvation. Additionally, the differentially short channel design suppresses along-the-channel effects.

Figure 1b shows the polarisation curve of the cell in H_2/H_2 operation. In this case the open circuit voltage is nearly 0 V. In the absence of CO in the whole current range the cell shows mainly ohmic behaviour caused by the membrane and other ohmic resistances. The polarisation curves in H_2/O_2 and H_2/H_2 operation clearly show that our experimental simplifications of avoided limiting behaviour and low cathode overpotential compared to H_2/O_2 operation are successfully achieved.

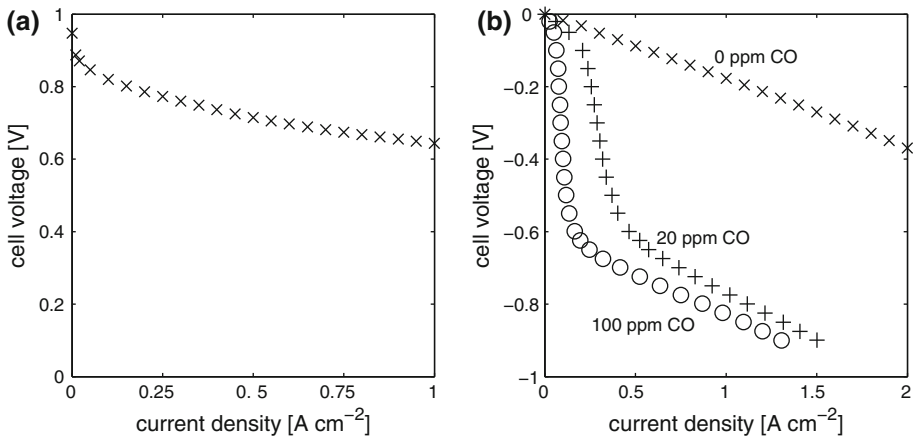

Fig. 1 Polarisation curve **a** in H_2/O_2 operation under normal conditions, **b** in H_2/H_2 operation with various anode CO content (*times* no CO, *plus* 20 ppm CO, *circle* 100 ppm CO)

If carbon monoxide is added to the anode gas, the polarisation curves show the features well known from literature [32, 33]. Especially, the typical S-shape profiles have been discussed by Camara et al. [34] and Lopes et al. [35]. In the case of 20 ppm CO small voltage losses are observed in the low current density region. In this region, active sites are blocked by CO for the hydrogen oxidation reaction, which causes the small voltage loss, but there are still enough active sites left for the hydrogen oxidation reaction. Then a steep voltage decline follows. The Tafel reaction becomes the rate determining step and defines a limiting current. The anode overpotential increases exponentially, until the onset potential for the CO oxidation is reached. Thus, the CO oxidation sets CO covered Pt sites free and increases the number of active sites for hydrogen oxidation. The polarisation curve levels off into an ohmic decrease at higher current densities, which is caused by membrane and ohmic losses. When the CO content is increased to 100 ppm the CO adsorption blocks more Pt sites and the limiting current, at which the steep voltage increase begins, is lower. Additionally, a slightly higher overpotential is necessary to free the surface from CO.

In Fig. 2 the EIS spectra of the cell at a working point of 0.1 A cm^{-2} is shown. This working point lies in the low current region, where the limiting current for hydrogen oxidation is not yet reached but the active area for this reaction is decreased by preferential adsorption of CO. This scenario represents the case of beginning CO poisoning before severe performance decrease is reached.

In the Nyquist plot in Fig. 2c it can be seen that the arc attributed to the Tafel Volmer reaction of hydrogen increases dramatically with increasing CO content. This increase in reaction resistance is caused by the decrease in active area available for the hydrogen oxidation reaction. This observation is in congruence with results from other groups [28, 36–39, 7].

The measured NFRA spectra are shown in Fig. 3. The first order frequency response function $H_{1,0}$ represents the linear behaviour of the cell. According to the mathematical background of the NFRA this function should be identical to the EIS spectra measured in the linear range with a small amplitude. This congruence is seen when comparing $H_{1,0}$ in Fig. 3a, b with the EIS spectra in Fig. 2a, b.

The $H_{1,0}$ spectrum of the H_2/H_2 cell without CO poisoning shows two time constants, which can be best identified in the Bode plot of the phase angle (Fig. 3b). As has been discussed by Ciureanu et al. [40, 28, 41], the first time constant in the range of 1 s (f = 1 Hz) can been attributed to the hydrogen chemisorption step of the Tafel Volmer mechanism. The second time constant lies in the range of 1 ms (f = 1 kHz) and can be attributed to the oxidation of the chemisorbed hydrogen, i.e. the Volmer step.

In the $H_{1,0}$ spectra under CO poisoning the high frequency time constant of the Volmer mechanism splits up into two time constants. Thereby, the high frequency time constant is caused by the fast Volmer step on a CO covered surface. At this high frequency, slower steps like adsorption can not follow the fast change of the input signal and the impedance is purely related to the electrooxidation step on a surface at steady state CO coverage. But the change of electrooxidation rate leads to a corresponding change in surface coverage of hydrogen. When the frequency is decreased, the CO adsorption can follow this change in surface coverage. With this, the hydrogen electrooxidation reaction takes place on a periodically changing surface area. This effect leads to the second time constant in the spectra. This explanation can also be supported by simulations from the model. In Fig. 4 the derivative of the CO coverage is set to zero in Eq. 13, i.e. the CO coverage is assumed to be fast and always in steady state. With this, the second time constant disappears and both time constants merge into one.

In the spectrum of 100 ppm an additional arc can be seen in the lower frequency end. This can be related to

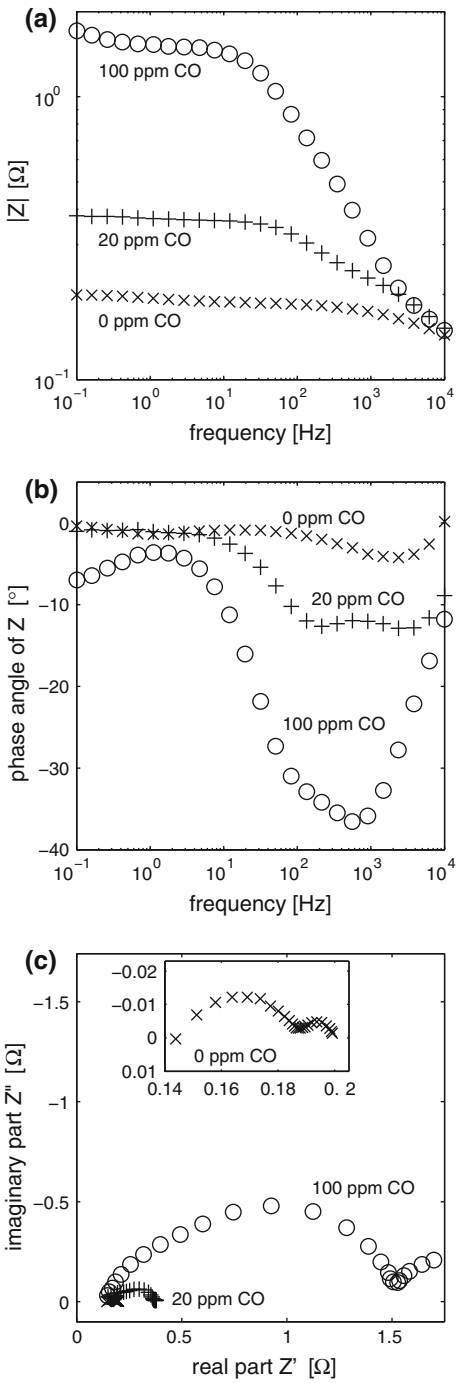

Fig. 2 Measured EIS spectra in H_2/H_2 operation with various anode CO content (*times* no CO, *plus* 20 ppm CO, *circle* 100 ppm CO). **a** Magnitude, **b** phase angle, **c** Nyquist plot of impedance, inset in **c** is a zoom of the spectrum without CO

beginning CO oxidation, which frees the surface and a new equilibrium coverage can be reached. Since the reaching of the equilibrium coverage due to the competing hydrogen and CO adsorption is the slowest process, this arc is seen in the lower frequency range.

Additional to the linear spectra, the second order function $H_{2,0}$ contains information about the nonlinearities of the cell. In Fig. 3c it can be seen that in the absence of CO the magnitude of $H_{2,0}$ is very low and not changing much. If the cell is poisoned by CO the magnitude increases in the low and middle frequency range. For high frequencies the magnitude is decreasing, whereby the decrease is steeper the higher the CO content is. The magnitude of the 100 ppm curve is even dropping below the 20 ppm curve. At the highest frequencies all curves level off in the same limiting value. The phase angle of $H_{2,0}$ in Fig. 3d shows a large change compared to the reference case without CO.

This features of the NFRA spectra might be used for a diagnosis of CO poisoning in PEMFC. In case of CO poisoning, the first harmonic shows a significant increase in magnitude and an enlargement of the semicircle attributed to the charge transfer reaction. Unfortunately, the same feature is seen in the case of dehydration, too [9]. This is because in both cases the active area available for the hydrogen oxidation reaction decreases, either by blockage due to CO or by partly inactivation of the catalyst by drying out of the Nafion network in the catalyst layer. Therefore, the increase of the linear reaction impedance is a necessary but not sufficient condition for the presence of CO poisoning. For a sufficient distinction between CO poisoning and dehydration, the second harmonic $H_{2,0}$ might be used. In case of CO poisoning, the most remarkable qualitative and quantitative feature of $H_{2,0}$ is the change of the phase angle towards lower frequencies.

4 Modelling

In this section, the experimental approach and the measurement results of the previous section shall be verified. To do so, a simple and well established model is taken from literature with its original parameters [31]. Using this model, the higher order frequency response functions are simulated and compared to the measurements. Thereby, the original parameters were not changed or fitted in order to validate the NFRA method. Also, the model was kept as simple as possible, on the one hand in order to preserve the possibility of an analytical derivation of the higher order frequency response functions. On the other hand, the simplicity of the model leads to spectra in which the main mechanisms are clearly visible although not every subprocess and intermediate step is represented in detail. Therefore, at the end of this section the model is reviewed critically and possibilities for refinement and extensions are given.

The current analysis used a fuel cell with a differentially short channel length, in which along-the-channel

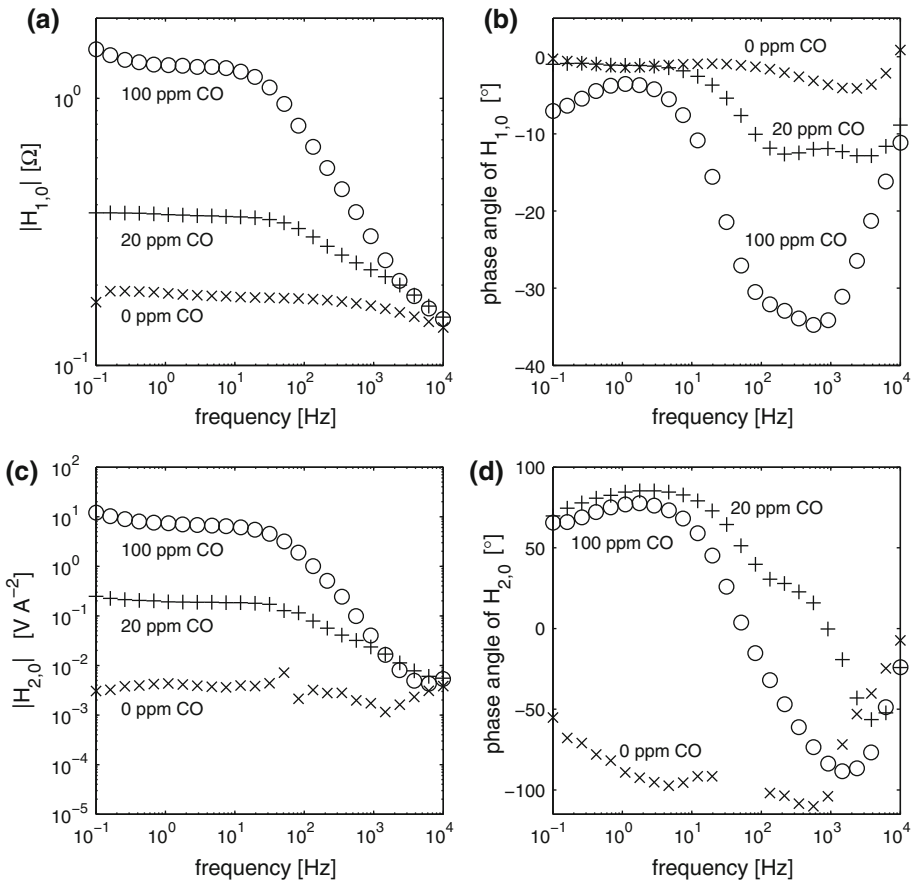

Fig. 3 Measured NFRA spectra in H_2/H_2 operation with various anode CO content (*times* no CO, *plus* 20 ppm CO, *circle* 100 ppm CO). **a** Magnitude of first order FRF $H_{1,0}$, **b** phase angle of first order FRF $H_{1,0}$, **c** magnitude of second order FRF $H_{2,0}$, and **d** phase angle of second order FRF $H_{2,0}$

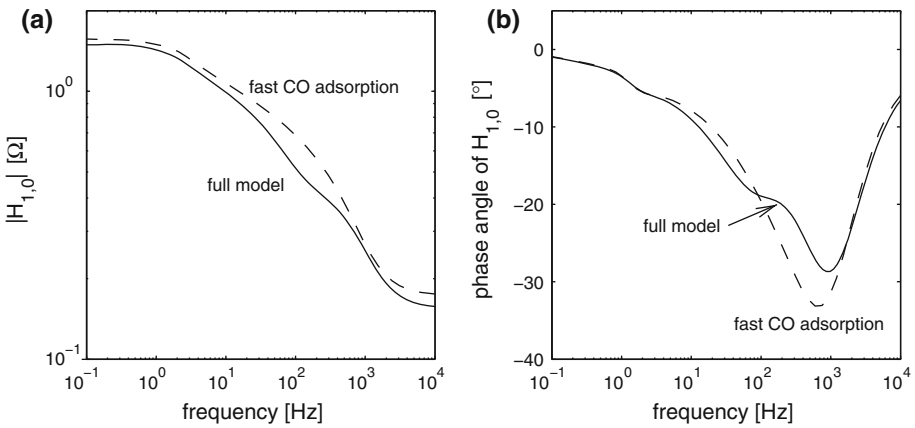

Fig. 4 Comparison of simulated NFRA spectra in H_2/H_2 operation with 100 ppm CO of the full model (*solid line*) and under the assumption of fast CO adsorption (*dashed line*). **a** Magnitude of first order FRF $H_{1,0}$, **b** phase angle of first order FRF $H_{1,0}$

distributions could be neglected. Therefore, the along-the-channel coordinate was neglected. Furthermore, the electrode was considered to be thin, mass transport resistances were neglected and isothermal conditions were assumed. Thus, a spatially lumped model was used. The cell voltage was calculated from anode and cathode overpotential and the voltage drop of the membrane. Anode and cathode overpotential were modelled with charge balance equations and reaction kinetics taken from literature [31]. The membrane was assumed to behave as an ohmic resistance.

Springer et al. [32, 31] suggested the following anode reaction scheme for a cell with CO poisoning:

$$\mathrm{H_2} + 2\mathrm{Pt} \underset{b_{fh} k_{fh}(\Theta_{\mathrm{CO}})}{\overset{k_{fh}(\Theta_{\mathrm{CO}})}{\rightleftharpoons}} 2(\mathrm{H}-\mathrm{Pt}) \tag{3}$$

$$(\mathrm{H}-\mathrm{Pt}) \overset{k_{eh}}{\rightarrow} \mathrm{Pt} + \mathrm{H}^+ + e^- \tag{4}$$

$$\mathrm{CO} + \mathrm{Pt} \underset{b_{fc}(\Theta_{\mathrm{CO}}) k_{fc}}{\overset{k_{fc}}{\rightleftharpoons}} \mathrm{CO}-\mathrm{Pt} \tag{5}$$

$$CO - Pt + H_2O \xrightarrow{k_{ec}} Pt + CO_2 + 2H^+ + 2e^- \quad (6)$$

At the cathode, the hydrogen reduction reaction takes place:

$$H^+ + e^- \xrightarrow{k_{eh}} 1/2H_2 \quad (7)$$

The electrical behaviour is described by charge balance equations for anode and cathode overpotential η_A and η_C, which are combined by Kirchhoff's voltage law to result in the cell voltage U_{cell}:

$$C_{DL,A}\frac{d\eta_A}{dt} = -Fr_{\mathrm{H}}^{ox} - 2Fr_{\mathrm{CO}}^{ox} + \frac{i}{\epsilon} \quad (8)$$

$$C_{DL,C}\frac{d\eta_C}{dt} = Fr_{\mathrm{H}}^{red} - \frac{i}{\epsilon} \quad (9)$$

$$U_{cell} = -\eta_A + \eta_C - iR_M \quad (10)$$

where $C_{DL,A}$ and $C_{DL,C}$ are anodic and cathodic double layer capacity in F m_{act}^{-2}, r_{H}^{ox} and r_{CO}^{ox} are the reaction rates of hydrogen and CO oxidation per active area in mol m_{act}^{-2} s^{-1}. Therefore, the current i is also normalized to the active area of the cell by means of a roughness factor ϵ in $m_{act}^2\, m_{geom}^{-2}$. By this normalization, the model is independent of the internal active surface area, a value which could not be determined exactly in our preparation method. The original kinetic parameters of Springer [31] could be used with the help of the conversion equations in Table 2. The difference in active surface area between our experiments and those of Springer were fixed by fitting the roughness factor ϵ in our model.

The membrane resistance R_M is determined from the relative humidity of the gases according to [42]:

$$R_M = \frac{d_M}{\kappa(a_{\mathrm{H_2O}})} = \frac{d_M}{1.3 \times 10^{-5} \exp\left(14a_{\mathrm{H_2O}}^{0.2}\right)} \quad (11)$$

where d_M is the thickness of the membrane and $a_{\mathrm{H_2O}}$ is the activity of the water vapour, i.e. the relative humidity as a value between 0 and 1.

The anode reaction kinetics are functions of the surface coverage of the platinum catalyst with hydrogen and carbon monoxide, Θ_H and Θ_{CO}. Material balances describe the temporal evolution of these surface coverages:

$$\rho\frac{d\Theta_{\mathrm{H}}}{dt} = r_{\mathrm{H}}^{ads} - r_{\mathrm{H}}^{des} - r_{\mathrm{H}}^{ox} \quad (12)$$

$$\rho\frac{d\Theta_{\mathrm{CO}}}{dt} = r_{\mathrm{CO}}^{ads} - r_{\mathrm{CO}}^{des} - r_{\mathrm{CO}}^{ox} \quad (13)$$

$$\Theta_{\mathrm{Pt}} = 1 - \Theta_{\mathrm{H}} - \Theta_{\mathrm{CO}} \quad (14)$$

where ρ is the number of active reaction sites per geometric area in mol m_{act}^{-2} and $r_{\mathrm{H/CO}}^{ads/des}$ are adsorption and desorption rates of hydrogen and carbon monoxide in mol m_{act}^{-2} s^{-1}. To describe the reaction rates at anode and cathode, Butler–Volmer kinetics with $\alpha = 0.5$ were assumed for hydrogen oxidation and Tafel kinetics were assumed for CO oxidation, according to [31]:

$$r_{\mathrm{H}}^{ox} = \Theta_{\mathrm{H}} k_{eh} 2\sinh\left(\frac{\eta_A}{b_h}\right) \quad (15)$$

$$r_{\mathrm{CO}}^{ox} = \Theta_{\mathrm{CO}} k_{ec} \exp\left(\frac{\eta_A}{b_c}\right) \quad (16)$$

$$r_{\mathrm{H}}^{red} = k_{eh} 2\sinh\left(\frac{\eta_C}{b_h}\right) \quad (17)$$

where b_h and b_c are the Tafel slope for hydrogen and CO oxidation, respectively. The hydrogen adsorption can be described with a Langmuir isotherm [31, 43]. The CO adsorption is described by a Temkin isotherm, according to [44, 45] and used in several modelling works [31, 43, 46].

$$r_{\mathrm{H}}^{ads} = k_{fh} x_{\mathrm{H}} p_A \Theta_{\mathrm{Pt}}^2 \quad (18)$$

$$r_{\mathrm{H}}^{des} = k_{fh} b_{fh} \Theta_{\mathrm{H}}^2 \quad (19)$$

$$r_{\mathrm{CO}}^{ads} = k_{fc} x_{\mathrm{CO}} p_A \Theta_{\mathrm{Pt}} \quad (20)$$

$$r_{\mathrm{CO}}^{des} = k_{fc} b_{fc} \Theta_{\mathrm{CO}} \quad (21)$$

where x_{H} and x_{CO} are the mole fraction of hydrogen gas and CO, p_A is the overall pressure of the anode. The CO adsorption-to-desorption ratio b_{fc} and hydrogen adsorption rate constant k_{fh} are a function of CO coverage [31]:

$$b_{fc}(\Theta_{\mathrm{CO}}) = b_{fc0} \exp\left(\Theta_{\mathrm{CO}} \frac{\delta(\Delta G_{\mathrm{CO}})}{RT}\right) \quad (22)$$

$$k_{fh}(\Theta_{\mathrm{CO}}) = k_{fh0} \exp\left[-\frac{\delta(\Delta E_H)}{RT}\left\{1 - \exp\left(-\frac{p\Theta_{\mathrm{CO}}}{1-\Theta_{\mathrm{CO}}}\right)\right\}\right] \quad (23)$$

where $\delta(\Delta G_{\mathrm{CO}})$ is the difference in adsorption free energy assumed between $\Theta_{\mathrm{CO}} = 1$ and $\Theta_{\mathrm{CO}} = 0$; $\delta(\Delta E_{\mathrm{H}})$ is the increase of the activation energy for dissociative chemisorption of H_2 if the neighbouring Pt catalyst site is covered with CO; p is the number of neighbouring Pt active sites. See the appendix B of [31] for further explanation and derivation of the Temkin adsorption behaviour.

Table 1 General cell parameters used in the model

	Used value	Reference
$a_{\mathrm{H_2O}}$	0.5445	
$C_{DL,A}$	984×10^{-6} F m_{act}^{-2}	Fitted
$C_{DL,C}$	984×10^{-6} F m_{act}^{-2}	Assumed
d_M	88.9×10^{-6} m	
p_A	101325 Pa	
T	358 K	
ρ	0.01042 mol m_{act}^{-2}	[46]
ϵ	0.663	Fitted

Table 2 Kinetic parameters of Springer et al. [31] and conversions used

	Used value	Conversion	Original value
b_c	0.06 V	No conversion	0.06 V
b_h	0.032 V	No conversion	0.032 V
b_{fc0}	1.5×10^{-3} Pa	Unit conversion	1.5×10^{-8} atm
b_{fh}	5.0662×10^{4} Pa	Unit conversion	0.5 atm
k_{ec}	5.1821×10^{-10} mol m_{act}^{-2} s^{-2}	$k_{ec} = k_{ec}^{*}/(\epsilon^{*}2F)$	10^{-8} A cm^{-2}
k_{eh}	0.4146 mol m_{act}^{-2} s^{-2}	$k_{eh} = k_{eh}^{*}/(\epsilon^{*}F)$	4 A cm^{-2}
k_{fc}	1.0229×10^{-5} mol m_{act}^{-2} s^{-2}	$k_{eh} = k_{eh}^{*}/(\epsilon^{*}F)$	10 A cm^{-2} atm^{-1}
k_{fh0}	4.0915×10^{-3} mol m_{act}^{-2} s^{-2}	$k_{eh} = k_{eh}^{*}/(\epsilon^{*}F)$	4000 A cm^{-2} atm^{-1}
p	5	No conversion	5
$\delta(\Delta G_{CO})/RT$	6.8	No conversion	6.8
$\delta(\Delta E_H)/RT$	4.6	No conversion	4.6

Asterisk in the conversion equations marks the original values

The parameters used for the modelling are given in Tables 1 and 2. The model has been implemented and solved in Matlab® Version 7.1.0.183. The NFRA spectra were simulated by in-house programmed Matlab® routines, which simulated the quasi-frequency response and calculated the HFRF in the same fashion as in the experiments, according to Eqs. 1 and 2.

From Fig. 5 it can be seen that the model describes the qualitative behaviour of the cell very good when compared to the measured spectra in Fig. 3. This shows that the model is valid in the dynamic and nonlinear range and might be used to derive NFRA spectra at different operation conditions.

Because of the simplicity of the model, on the one hand the NFRA spectra can be determined numerically and a screening of parameters can be used to analyse the influence of each parameter or process on the NFRA spectra. On the other hand, an analytical solution of the NFRA spectra can be derived. These can be analysed mathematically on the one hand to find out which parameters have a

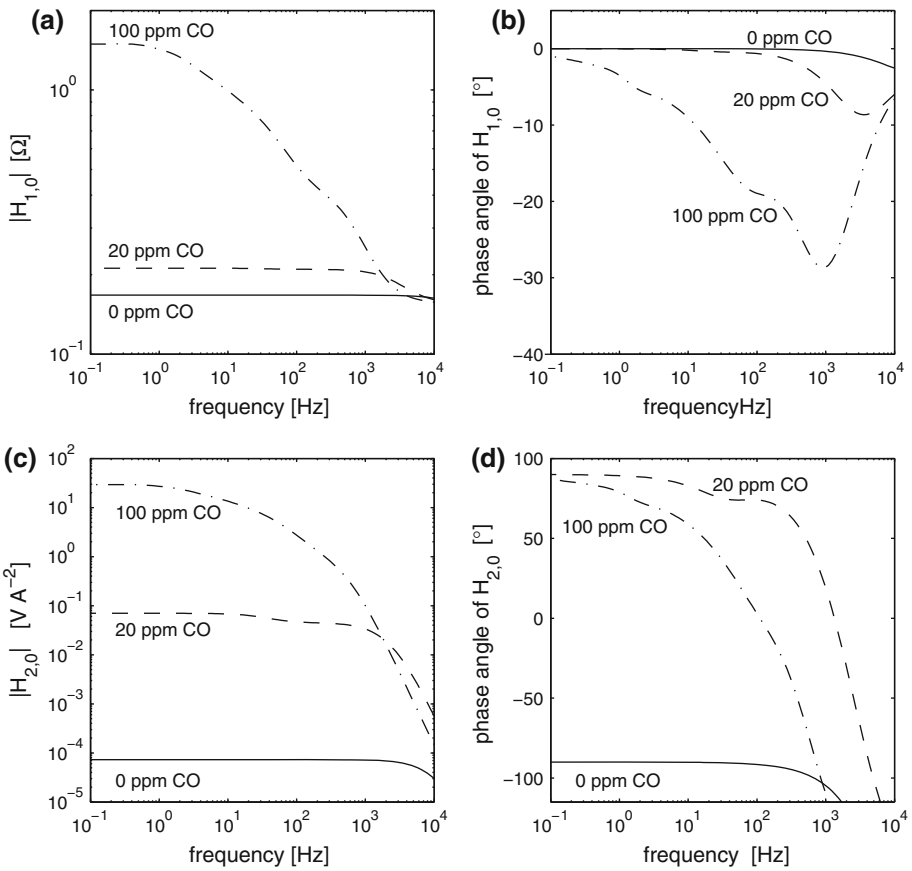

Fig. 5 Simulated NFRA spectra in H_2/H_2 operation with various anode CO content (*solid line* no CO, *dashed line* 20 ppm CO, *dash dotted line* 100 ppm CO). **a** Magnitude of first order FRF $H_{1,0}$, **b** phase angle of first order FRF $H_{1,0}$, **c** magnitude of second order FRF $H_{2,0}$, **d** phase angle of second order FRF $H_{2,0}$

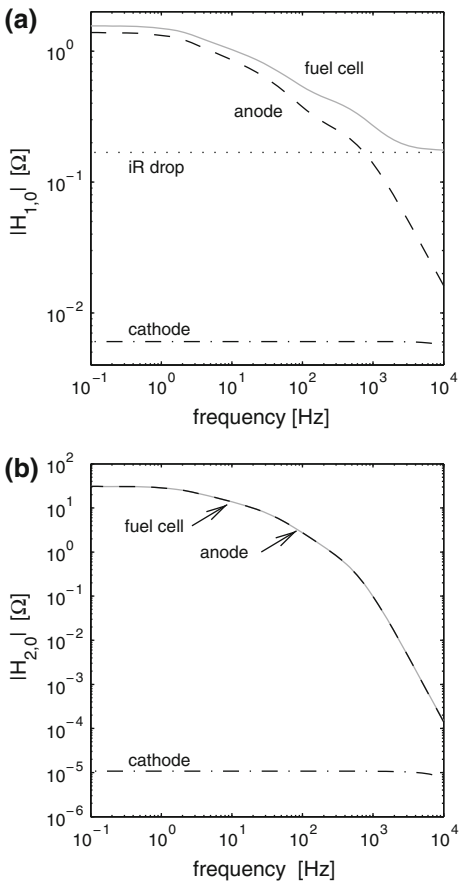

Fig. 6 Simulated NFRA spectra at 0.1 A cm^{-2} and 100 ppm CO of the whole cell (*gray*), anode (*dashed line*), cathode (*dash-dotted line*) and membrane and ohmic resistances (*dotted line*). **a** Magnitude of first order FRF $H_{1,0}$ (logarithmic scale), **b** magnitude of second order FRF $H_{2,0}$ (logarithmic scale). Note that in **b** the spectra of the whole cell and of the anode overlap and that the values of the membrane and ohmic resistances are below 10^{-15} Ω, i.e. in the range of numerical noise and practically zero

strong influence on the spectra and which are the governing processes. On the other hand, domains in the spectra can be found which are sensitive towards single processes. These domains might allow an unambiguous diagnosis of performance lowering processes.

Nevertheless, the model strongly simplifies the anode and cathode reactions. At the anode, the CO oxidation (Eq. 6) is modelled as one overall electro-oxidation reaction via water, although several elementary steps are possible [47–50]:

$$CO - Pt + H_2O - Pt \rightarrow CO_2 + H_2 + 2Pt \quad (24)$$

$$CO - Pt + O - Pt \rightarrow CO_2 + H_2 + 2Pt \quad (25)$$

$$CO - Pt + OH - Pt \rightarrow CO_2 + H^+ + e^- + 2Pt \quad (26)$$

$$H_2O + Pt \rightleftharpoons OH - Pt + H^+ + e^- \quad (27)$$

Equation 26 describes the water–gas-shift (WGS) reaction, which might be neglected at low temperatures in PEMFC. Equation 27 describes the direct oxidation of CO with oxygen either present in the fuel gas ("air-bleed") [47] or from diffusion from the cathode side through the membrane [48]. This reaction can be excluded because in the current experiments in H_2/H_2 operation no molecular oxygen is present. Therefore, the dominating reaction for CO oxidation is probably the electro-oxidation of CO with adsorbed OH (Eq. 28) stemming from a water dissociation step (Eq. 28) [51]. Note that although the water dissociation reaction (Eq. 28) was originally proposed for PtRu catalyst, it was recently shown by an analysis of autonomous oscillations in PEMFC that this step is also likely to take place at pure Pt but at higher overpotentials [52].

Additionally, the hydrogen oxidation mechanism of the model might not be sufficient for all operation conditions. At high overpotentials the Heyrovský reaction [53], i.e. an electrochemical hydrogen adsorption step, is likely to take place [54]:

$$H_2 + Pt \rightarrow Pt - H + H^+ + e^- \quad (28)$$

This reaction becomes dominating when most of the surface is blocked by CO ($\Theta_{CO} > 0.6$ [55]) and the overpotential reaches high values. Nevertheless, the current measurements were carried out at low overpotentials in a scenario of beginning CO poisoning, as explained in Sect. 3. If the high potential region should be included, dual pathway kinetic models as suggested in Ref. [54, 56] might be used.

The cathode is modelled in a very simple way in order to keep the model as simple as possible. Because of the large exchange current density of the cathodic hydrogen evolution reaction, the cathode can be seen as a pseudo-reference electrode of nearly constant potential [57]. Therefore, the cathode has no significant influence on the determined spectra. This can be additionally seen in Fig. 6, where the fraction of anode, cathode and membrane on the first and second harmonic are shown; the fraction of the cathode on first and second harmonic are negligibly small.

5 Conclusions

The influence of carbon monoxide on the NFRA spectra of a PEMFC were investigated in a tailored experimental setup. Therefore, a differential fuel cell design was used to avoid spatial distributions along the channel. H_2/H_2 operation eliminated the masking effect of the cathode and avoided possible side reactions of molecular oxygen. Polarisation curves and EIS spectra were used to verify this experimental approach.

With this setup, Nonlinear Frequency Response Analysis (NFRA) spectra were measured at different CO concentrations at a working point simulating a scenario of

beginning CO poisoning. Therefore, the measured spectra showed features which are relevant for a diagnosis of beginning CO poisoning during normal fuel cell operation. A concrete strategy using these features was suggested.

Finally, the NFRA approach was completed by a simple model from literature [31]. Simulations using the original model parameters resulted in NFRA spectra in reasonably good agreement with the measured spectra. This comparison validated the experimental approach as well as the theoretical simplifications of the model on the one hand. On the other hand the model was simple enough to allow a analytical derivation of the NFRA spectra and a theoretical evaluation of these. Nevertheless, the model was reviewed critically and simplifications and limitations were explained and validated. Suggestions for refinement and extensions of the model were given.

References

1. Bessarab Y, Merfert I, Fischer W, Lindemann A (2008) Different control methods of bidirectional DC–DC converters for fuel cell power systems. In: PCIM Europe 2008. International exhibition and conference for power electronics intelligent motion power quality. Mesago PCIM GmbH, Stuttgart, Germany, p 5
2. Bard AJ, Faulkner LR (2001) Electrochemical methods: fundamentals and applications, 2nd edn. Wiley, New York
3. Barsoukov E, MacDonald JR (2005) Impedance spectroscopy: theory, experiment, and applications, 2nd edn. John Wiley and Sons, New York
4. Orazem ME, Tribollet B (2008) Electrochemical impedance spectroscopy. The electrochemical society series, vol 48. Wiley-Interscience, New York
5. Yuan XZ, Song C, Wang H, Zhang J (2009) Electrochemical impedance spectroscopy in PEM fuel cells: fundamentals and applications. Springer, New York
6. Fouquet N, Doulet C, Nouillant C, Dauphin-Tanguy G, Ould-Bouamama B (2006) Model based PEM fuel cell state-of-health monitoring via AC impedance measurements. J Power Sources 159(2):905–913
7. Le Canut JM, Abouatallah RM, Harrington DA (2006) Detection of membrane drying, fuel cell flooding, and anode catalyst poisoning on PEMFC stacks by electrochemical impedance spectroscopy. J Electrochem Soc 153(5):A857–A864
8. Merida W, Harrington DA, Le Canut JM, McLean G (2006) Characterisation of proton exchange membrane fuel cell (PEMFC) failures via electrochemical impedance spectroscopy. J Power Sources 161(1):264–274
9. Kadyk T, Hanke-Rauschenbach R, Sundmacher K (2009) Nonlinear frequency response analysis of PEM fuel cells for diagnosis of dehydration, flooding and CO-poisoning. J Electroanal Chem 630:19–27
10. Engblom SO, Myland JC, Oldham KB (2000) Must AC voltammetry employ small signals? J Electroanal Chem 480(1–2): 120–132
11. Gavaghan DJ, Bond AM (2000) A complete numerical simulation of the techniques of alternating current linear sweep and cyclic voltammetry: analysis of a reversible process by conventional and fast fourier transform methods. J Electroanal Chem 480(1–2): 133–149
12. Smith DE (1966) Electroanalytical chemistry: a series of advances. Marcel Dekker, New York
13. Jankowski J (2002) Electrochemical methods for corrosion rate determination under cathodic polarisation conditions—a review part 2: AC methods. Corros Rev 20(3):179–200
14. Darowicki K, Majewska J (1999) Harmonic analysis of electrochemical and corrosion systems—a review. Corros Rev 17(5–6):383–399
15. Groysman A (2009) Corrosion monitoring. Corros Rev 27(4–5): 205–343
16. Mao Q, Krewer U, Hanke-Rauschenbach R (2010) Total harmonic distortion analysis for direct methanol fuel cell anode. Electrochem Commun 12:1517–1519
17. Mao Q, Krewer U, Hanke-Rauschenbach R (2011) Comparative studies on linear and nonlinear frequency response for direct methanol fuel cell anode. Submitted to J Electrochem Soc
18. Bensmann B, Petkovska M, Vidaković-Koch T, Hanke-Rauschenbach R, Sundmacher K (2010) Nonlinear frequency response of electrochemical methanol oxidation kinetics: a theoretical analysis. J Electrochem Soc 157(9):B1279–B1289
19. Darowicki K (1994) Fundamental-harmonic impedance of 1st-order electrode-reactions. Electrochim Acta 39(18):2757–2762
20. Darowicki K (1995) Corrosion rate measurements by nonlinear electrochemical impedance spectroscopy. Corros Sci 37(6):913–925
21. Darowicki K (1995) The amplitude analysis of impedance spectra. Electrochim Acta 40(4):439–445
22. Wilson JR, Schwartz DT, Adler SB (2006) Nonlinear electrochemical impedance spectroscopy for solid oxide fuel cell cathode materials. Electrochim Acta 51(8–9):1389–1402
23. Wilson JR, Sase M, Kawada T, Adler SB (2007) Measurement of oxygen exchange kinetics on thin-film La0.6Sr0.4CoO3-delta using nonlinear electrochemical impedance spectroscopy. Electrochem Solid State Lett 10(5):B81–B86
24. Weiner DD, Spina JF (1980) Sinusoidal analysis and modeling of weakly nonlinear circuits. Van Nostrand Reinhold Company, New York
25. Petkovska M (2006) Nonlinear frequency response method for investigation of equilibria and kinetics of adsorption systems. In: Spasic AM, Hsu J-P (eds) Finely dispersed particles—micro-, nano-, and atto-engineering, chap. 12. CRC Press, Boca Raton, pp 283–328
26. Petkovska M, Do DD (2000) Use of higher-order frequency response functions for identification of nonlinear adsorption kinetics: single mechanisms under isothermal conditions. Nonlinear Dyn 21(4):353–376
27. Wagner N, Schnurnberger W, Müller B, Lang M (1998) Electrochemical impedance spectra of solid-oxide fuel cells and polymer membrane fuel cells. Electrochim Acta 43(24):3785–3793
28. Ciureanu M, Wang H (1999) Electrochemical impedance study of electrode-membrane assemblies in PEM fuel cells I. Electro-oxidation of H_2 and H_2/CO mixtures on Pt-based gas-diffusion electrodes. J Electrochem Soc 146(11):4031–4040
29. Himanen O, Hottinen T, Mikkola M, Saarinen V (2006) Characterization of membrane electrode assembly with hydrogen–hydrogen cell and AC-impedance spectroscopy part I: Experimental. Electrochim Acta 52(1):206–214
30. Schneider IA, von Dahlen S, Wokaun A, Scherer GG (2010) A segmented microstructured flow field approach for submillimeter resolved local current measurement in channel and land areas of a PEFC. J Electrochem Soc 157(3):B338–B341
31. Springer TE, Rockward T, Zawodzinski TA, Gottesfeld S (2001) Model for polymer electrolyte fuel cell operation on reformate feed-effects of CO, H_2 dilution, and high fuel utilization. J Electrochem Soc 148(1):A11–A23

32. Springer TE, Zawodzinski TA, Gottesfeld S (1997) Modelling of polymer electrolyte fuel cell performance with reformate feed streams: effects of low levels of CO in hydrogen. In: McBreen J, Muckerjee S, Srinivasan S (eds) Electrode materials and processes for energy conversion and storage. The electrochemical society proceedings, vol 97. The Electrochemical Society, Pennington, pp 15–24
33. Lee SJ, Mukerjee S, Ticianelli EA, McBreen J (1999) Electrocatalysis of CO tolerance in hydrogen oxidation reaction in PEM fuel cells. Electrochim Acta 44(19):3283–3293
34. Camara GA, Ticianelli EA, Mukerjee S, Lee SJ, McBreen J (2002) The CO poisoning mechanism of the hydrogen oxidation reaction in proton exchange membrane fuel cells. J Electrochem Soc 149(6):A748–A753
35. Lopes PP, Ticianelli EA (2010) The CO tolerance pathways on the Pt-Ru electrocatalytic system. J Electroanal Chem 644(2): 110–116
36. Kim JD, Park YI, Kobayashi K, Nagai M, Kunimatsu M (2001) Characterization of CO tolerance of PEMFC by AC impedance spectroscopy. Solid State Ion 140(3-4):313–325
37. Kim JD, Park YI, Kobayashi K, Nagai M (2001) Effect of CO gas and anode-metal loading on H_2 oxidation in proton exchange membrane fuel cell. J Power Sources 103(1):127–133
38. Wagner N, Schulze M (2003) Change of electrochemical impedance spectra during CO poisoning of the Pt and Pt-Ru anodes in a membrane fuel cell (PEFC). Electrochim Acta 48(25–26):3899–3907
39. Wagner N, Gülzow E (2004) Change of electrochemical impedance spectra (EIS) with time during CO-poisoning of the Pt-anode in a membrane fuel cell. J Power Sources 127(1–2):341–347
40. Ciureanu M, Wang H (2000) Electrochemical impedance study of anode CO-poisoning in PEM fuel cells. J New Mater Electrochem Syst 3(2):107–119
41. Ciureanu M, Wang H, Qi ZG (1999) Electrochemical impedance study of membrane-electrode assemblies in PEM fuel cells: II. Electrooxidation of H_2 and H_2/CO mixtures on Pt/Ru-based gas-diffusion electrodes. J Phys Chem B 103(44):9645–9657
42. Yang C, Srinivasan S, Bocarsly AB, Tulyani S, Benziger JB (2004) A comparison of physical properties and fuel cell performance of Nafion and Zirconium Phosphate/Nafion composite membranes. J Membr Sci 237(1–2):145–161
43. Baschuk JJ, Li XG (2003) Modelling CO poisoning and O_2 bleeding in a PEM fuel cell anode. Int J Energy Res 27(12):1095–1116
44. Adamson AW (1967) Physical chemistry of surfaces. Interscience, New York
45. Dhar HP, Christner LG, Kush AK (1987) Nature of CO adsorption during H_2 oxidation in relation to modelling for CO poisoning of a fuel-cell anode. J Electrochem Soc 134(12):3021–3026
46. Shah AA, Sui PC, Kim GS, Ye S (2007) A transient PEMFC model with CO poisoning and mitigation by O2 bleeding and Ru-containing catalyst. J Power Sources 166(1):1–21
47. Gottesfeld S, Pafford J (1988) A new approach to the problem of carbon-monoxide poisoning in fuel-cells operating at low-temperatures. J Electrochem Soc 135(10):2651–2652
48. Zhang JX, Thampan T, Datta R (2002) Influence of anode flow rate and cathode oxygen pressure on CO poisoning of proton exchange membrane fuel cells. J Electrochem Soc 149(6):A765–A772
49. Zhang JX, Datta R (2005) Electrochemical preferential oxidation of CO in reformate. J Electrochem Soc 152(6):A1180–A1187
50. Ioroi T, Akita T, Yamazaki S, Siroma Z, Fujiwara N, Yasuda K (2006) Comparative study of carbon-supported Pt/Mo-oxide and PtRu for use as CO-tolerant anode catalysts. Electrochim Acta 52(2):491–498
51. Zhang JX, Datta R (2002) Sustained potential oscillations in proton exchange membrane fuel cells with PtRu as anode catalyst. J Electrochem Soc 149(11):A1423–A1431
52. Kadyk T, Kirsch S, Hanke-Rauschenbach R, Sundmacher K (2011) Autonomous potential oscillations at the Pt anode of a PEM fuel cell under CO poisoning. Submitted to Electrochim Acta
53. Heyrovský J (1927) A theory of overpotential. Recl Trav Chim Pays-Bas 46:582–585
54. Wang JX, Springer TE, Adzic RR (2006) Dual-pathway kinetic equation for the hydrogen oxidation reaction on Pt electrodes. J Electrochem Soc 153:A1732–A1740
55. Elezović NR, Gajic-Krstajic L, Radmilovic V, Vracar L, Krstajic NV (2009) Effect of chemisorbed carbon monoxide on Pt/C electrode on the mechanism of the hydrogen oxidation reaction. Electrochim Acta 54(4):1375–1382
56. Vilekar SA, Fishtik I, Datta R (2010) Kinetics of the hydrogen electrode reaction. J Electrochem Soc 157(7):B1040–B1050
57. Newman JS (1991) Electrochemical systems, chap 5, 2nd edn. Prentice-Hall, New Jersey, pp 116–133